Appl. Phys. B 62, 339–344 (1996)

Applied Physics B Lasers and Optics

Excited-state absorption in Er:BaY_2F_8 and $Cs_3Er_2Br_9$ and comparison with Er:$LiYF_4$

M. Pollnau[1], W. Lüthy[1], H. P. Weber[1], K. Krämer[2], H. U. Güdel[2], R. A. McFarlane[3]

[1] Institute of Applied Physics, University of Berne, Sidlerstrasse 5, CH-3012 Berne, Switzerland
(Fax: + 41-31/631-3765, E-mail: POLLNAU@iap.unibe.ch)
[2] Institute of Inorganic Chemistry, University of Berne, Freiestrasse 3, CH-3009 Berne, Switzerland
[3] Hughes Research Laboratories, 3011 Malibu Canyon Road, Malibu, CA 90265, USA

Received: 6 July 1995/Accepted: 12 September 1995

Abstract. The influence of Excited-State Absorption (ESA) on the green laser transition and the overlap of Ground-State Absorption (GSA) and ESA for 970 nm upconversion pumping in erbium is investigated in Er^{3+}: BaY_2F_8 and $Cs_3Er_2Br_9$. Results are compared to Er^{3+}: $LiYF_4$. In Er^{3+}: BaY_2F_8, a good overlap between GSA and ESA is found at 969 nm in one polarization direction. The emission cross section at 550 nm is a factor of two smaller than in $LiYF_4$. In $Cs_3Er_2Br_9$, the smaller Stark splitting of the levels shifts the wavelengths of the green emission and ESA from $^4I_{13/2}$ off resonance. It enhances, however, ground-state reabsorption. The emission cross section at 550 nm is comparable to $LiYF_4$. Upconversion leads to significant green fluorescence from $^2H_{9/2}$. A significant population of the $^4I_{11/2}$ level and ESA at 970 nm are not present under 800 nm pumping.

PACS: 42.55.Rz; 42.60.Lh; 78.45. + h

The development of compact blue and green crystal lasers pumped by infrared diodes is of interest today for applications in the fields of data storage and display. Green laser emission in erbium-doped crystals at cryogenic temperatures [1–4] has stimulated further investigations of this system. Efficient room-temperature lasing has been reported in Er^{3+} (1%):$LiYF_4$ so far [5, 6]. A detrimental effect to green emission, however, is the reabsorption of laser light by Excited-State Absorption (ESA) from the $^4I_{13/2}$ level. This effect has been shown to prevent room-temperature lasing in Er^{3+}:$YAlO_3$ [7]. In $LiYF_4$ the 551 nm emission peak is, in contrast to $YAlO_3$, located between two ESA peaks [8] and reabsorption has only a small practical influence [9].

In other crystals the green laser may suffer from the same negative effects as in $YAlO_3$. The search for new host materials for green laser emission, therefore, has to include the measurement of ESA at the wavelengths of the green emission. Also a good overlap of Ground-State Absorption (GSA) and ESA at 970 nm [6] is of interest for efficient laser-diode upconversion-pumped operation.

The BaY_2F_8 and $Cs_3Er_2Br_9$ crystals which are investigated and compared to $LiYF_4$ in this paper are interesting candidates as host materials for green laser emission. Phonon energies of 415 cm^{-1} in BaY_2F_8 [10] and 190 cm^{-1} in $Cs_3Er_2Br_9$ [11] lead to a long lifetime of the $^4S_{3/2}$ upper laser level. The measurement of GSA, ESA, and fluorescence provides important information on the conditions for possible upconversion-pumped room-temperature lasing in BaY_2F_8 and $Cs_3Er_2Br_9$. Owing to different size and weight of the ligands, the excitation mechanisms, fluorescence properties, ESA and Stimulated-Emission (SE) dynamics are completely different in the bromide compared to the fluoride materials. Systematic changes and their impact on green laser emission are discussed.

1 Experimental

A pump- and probe-beam technique is used for the measurement of quasi-cw-pumped ESA spectra, see Fig. 1. The experimental arrangement is similar to those used in [8, 12, 13]. The sample is placed in front of a pinhole of 300 μm diameter in order to ensure a good overlap between pump and probe beam. The sample is excited at 800 nm with an Ar^+-laser-pumped Ti:sapphire laser of 200 mW. Broadband probe light from a 250 W halogen lamp is focused into the sample. The transmitted probe-beam spectrum passes through a monochromator (1.15 m spectrometer, resolution 0.2 nm) and is detected with an optical photodiode. The probe light is chopped with a frequency of 390 Hz and amplified in lock-in technique to avoid the detection of scattered pump light and fluorescence from the sample. The pump beam is chopped with 11 Hz. With a second lock-in amplifier set at 11 Hz the difference $\Delta I = I_p - I_u$ between the transmitted probe-beam intensities I_p and I_u in the pumped and unpumped case is amplified [8, 12, 13] and recorded on a PC. The probe-beam intensities I_u transmitted through the unpumped sample and I_0 without a sample are measured in lock-in

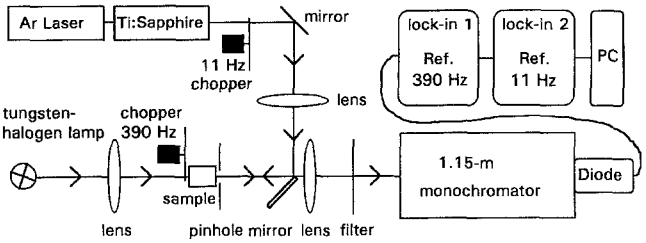

Fig. 1. Experimental arrangement for the measurement of ESA

technique at the frequency of the probe-beam chopper reference. With n_0, the dopant concentration, and d, the thickness of the sample, the GSA cross section σ_{GSA} is determined from the Lambert-Beer law

$$\sigma_{GSA} = \ln(I_0/I_u)/(n_0 d). \tag{1}$$

With the approximation

$$-(\Delta I/I_u) = (I_u - I_p)/I_u \approx \ln(I_u/I_p), \tag{2}$$

the diff-erences in cross sections σ of ESA and SE originating from level i at wavelength λ are calculated from the measured quantities using the equation [14]

$$\sum_i [(n_i/n_e)(\sigma_{ESA,i} - \sigma_{SE,i})] = \ln(I_u/I_p)/(n_e d) + \sigma_{GSA}. \tag{3}$$

The sum in (3) extends over all metastable levels which have a substantial relative population density n_i/n_e. The excitation density n_e is determined at wavelengths where the bleaching of GSA but no ESA or SE occurs [14]. At these wavelengths (3) reduces to

$$\ln(I_u/I_p)/(n_e d) + \sigma_{GSA} = 0. \tag{4}$$

The parameter n_e is determined correctly if the measured bleaching of the GSA in the $\ln(I_u/I_p)$ spectrum is compensated by the addition of the GSA spectrum in (4). The obtained value of n_e includes the amplification factor of the lock-in technique [8]. The ESA and SE transitions measured at other wavelengths are amplified in the same way as the bleaching of the GSA. Thus the ESA and SE cross sections obtained from (3) with the value of n_e determined from (4) are correct. The measurement of $\ln(I_u/I_p)$ and σ_{GSA} in the same experimental arrangement ensures the same spectral resolution and allows the correct addition of both spectra in (3). The fluorescence spectra are also measured with this arrangement and the same spectral resolution with a normal lock-in technique using the frequency of the pump-beam chopper as the reference. Emission cross sections are calibrated in the same way as in [7].

For the correction of the measured $\ln(I_u/I_p)$ spectrum a careful analysis is necessary. The calculated ESA/SE spectrum obtained from (3) does not contain GSA transitions. It does, however, contain SE transitions into the ground state. A higher transmission of the probe light at the wavelengths of GSA transitions in the pumped compared to the unpumped case occurs owing to two effects: a smaller GSA due to the bleaching of the ground state and SE due to the population of the excited state. After the elimination of the ground-state bleaching from the $\ln(I_u/I_p)$ spectrum the SE remains. The determined SE cross section from level i is the atomic cross section of the Stark transition times the Boltzmann factor of the initial Stark level times the fraction n_i/n_e of the whole excitation n_e. This SE does not imply and must not be confused with population inversion on the measured transition. If a broadband ESA/SE spectrum is investigated several GSA transitions may be found that terminate in short-living excited states and that do not suffer from ESA at the same wavelengths [14]. The relative populations n_i/n_e of these excited states are small and no SE is measured. The correction of the $\ln(I_u/I_p)$ spectrum towards zero at these wavelengths leads to the correct ESA and SE cross sections in the whole spectrum. In this publication narrow wavelength ranges are investigated with high resolution. Only the bleaching of the GSA transition into the $^4I_{11/2}$ or $^4S_{3/2}$ level of erbium is detected. Both levels are populated to a considerable fraction n_i/n_e of the excitation n_e and, therefore, SE into the ground state is present in the calculated spectra.

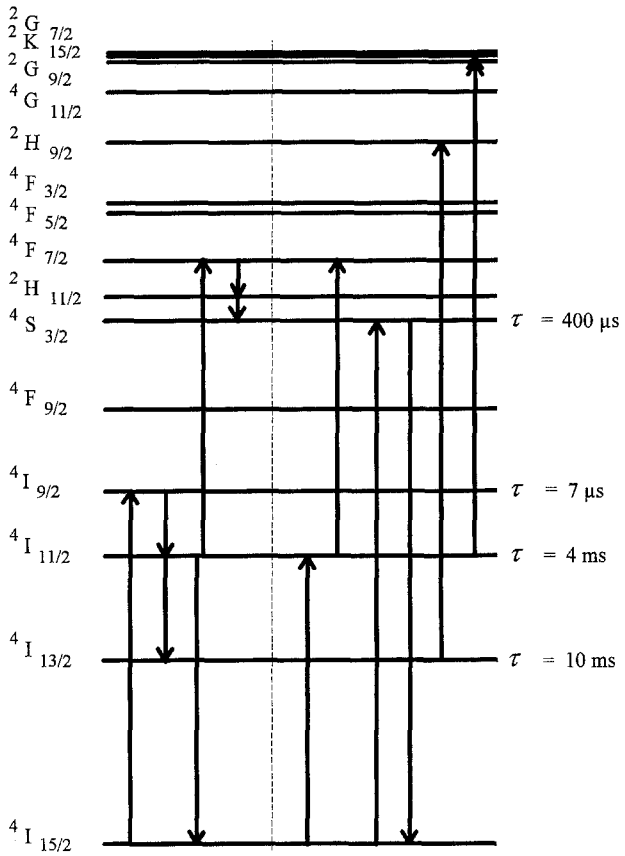

Fig. 2. Energy-level diagram indicating the excitation mechanisms (*left-hand side*) and the detected transitions (*right-hand side*) in Er(5%): $LiYF_4$ and Er(7.5%): BaY_2F_8. The erbium ions are excited into the $^4I_{9/2}$ level. Multiphonon relaxations populate the $^4I_{11/2}$ and $^4I_{13/2}$ levels. Interionic upconversion and multiphonon relaxations populate the $^4S_{3/2}$ level. Investigated are the overlap of GSA to $^4I_{11/2}$ and ESA from $^4I_{11/2}$ at the pump wavelength 970 nm as well as the overlap of GSA to $^4S_{3/2}$, fluorescence from $^4S_{3/2}$, and ESA from $^4I_{13/2}$ and $^4I_{11/2}$ at the laser wavelength 550 nm

2 Results

The energy level scheme of erbium, the intrinsic lifetimes of the various metastable levels in the different host materials, the excitation mechanisms under 800 nm radiation, and the investigated transitions are indicated in Fig. 2 for BaY_2F_8 and $LiYF_4$. The indicated lifetimes are the intrinsic lifetimes of the system at low dopant concentration and include radiative as well as multiphonon relaxations. The $LiYF_4$ lifetimes given in Fig. 2 are mean values of data published for 1% erbium concentration, e.g., in [5, 10, 15]. In BaY_2F_8 the corresponding lifetimes for 1% erbium concentration [10] are 630 µs ($^4S_{3/2}$), 9.6 ms ($^4I_{11/2}$), and 10.6 ms ($^4I_{13/2}$). In $Cs_3Er_2Br_9$ completely different excitation mechanisms are active and different transitions are detected, as shown in Fig. 3. The indicated intrinsic lifetimes [16] were measured in $Er^{3+}(1\%):Cs_3Lu_2Br_9$.

With the technique described in Sect. 1 the overlap of GSA $^4I_{15/2} \rightarrow {}^4I_{11/2}$ and ESA $^4I_{11/2} \rightarrow {}^4F_{7/2}$ for laser-diode upconversion pumping at the wavelength 970 nm as well as the influence of GSA $^4I_{15/2} \rightarrow {}^4S_{3/2}$ and parasitic ESA $^4I_{13/2} \rightarrow {}^2H_{9/2}$ and $^4I_{11/2} \rightarrow {}^2K_{15/2} + {}^2G_{9/2}$ on the emission $^4S_{3/2} \rightarrow {}^4I_{15/2}$ at the laser wavelength 550 nm are investigated. The originating levels of the different ESA transitions around 550 nm are known from time-resolved ESA measurements in $Er^{3+}:YAlO_3$ [7, 14]. Their wavelength ranges and cross sections do not change dramatically in BaY_2F_8 and $LiYF_4$ in contrast to $Cs_3Er_2Br_9$.

The GSA and ESA spectra at the pump wavelength 970 nm are shown for BaY_2F_8 (Fig. 4) and $LiYF_4$ (Fig. 5). The overlap of GSA and ESA is different for the two investigated polarization directions. Spectra of $LiYF_4$ with lower spectral resolution have earlier been presented in [8]. In Fig. 6 the GSA, fluorescence, and ESA spectra of BaY_2F_8 and $LiYF_4$ at the laser wavelength 550 nm are compared for the polarization directions **E**‖**y** in BaY_2F_8 and **E**‖**c** in $LiYF_4$. Qualitative behaviour and wavelengths are comparable for **E**‖**z** in BaY_2F_8 and **E**‖**a** in $LiYF_4$, but absorption and emission cross sections are smaller. The same spectra of $Cs_3Er_2Br_9$ are given in Fig. 7 for arbitrary polarization, because the investigated sample is unoriented.

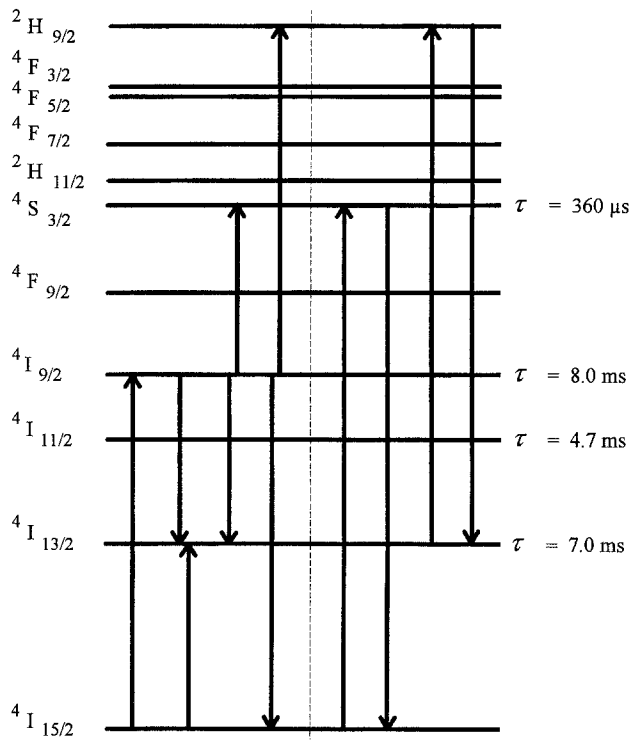

Fig. 3. Energy-level diagram indicating the excitation mechanisms (*left-hand side*) and the detected transitions (*right-hand side*) in $Cs_3Er_2Br_9$. The erbium ions are excited into the $^4I_{9/2}$ level. Cross-relaxation and upconversion processes from $^4I_{9/2}$ populate the $^4I_{13/2}$ level. Upconversion processes from $^4I_{9/2}$ populate the $^4S_{3/2}$ and $^2H_{9/2}$ levels. The $^4I_{11/2}$ level is not significantly populated under excitation at 800 nm. Investigated is the overlap of GSA to $^4S_{3/2}$, fluorescence from $^4S_{3/2}$, ESA from $^4I_{13/2}$, and fluorescence from $^2H_{9/2}$ at the possible laser wavelength 550 nm

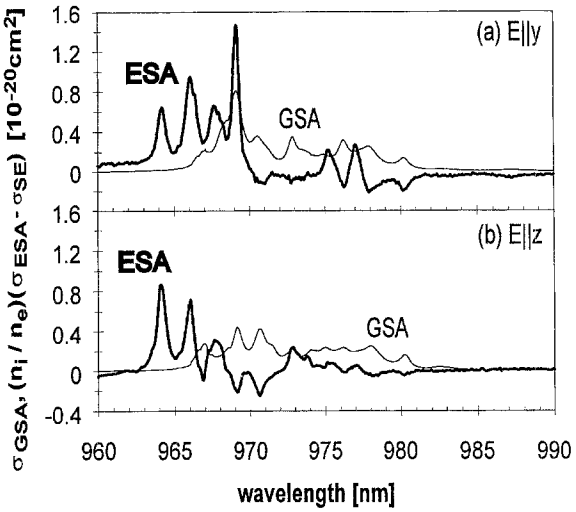

Fig. 4a, b. Polarized spectra at the pump wavelength 970 nm of $Er(7.5\%):BaY_2F_8$, (**a**) **E**‖**y**, (**b**) **E**‖**z**: GSA $^4I_{15/2} \rightarrow {}^4I_{11/2}$ and ESA $^4I_{11/2} \rightarrow {}^4F_{7/2}$

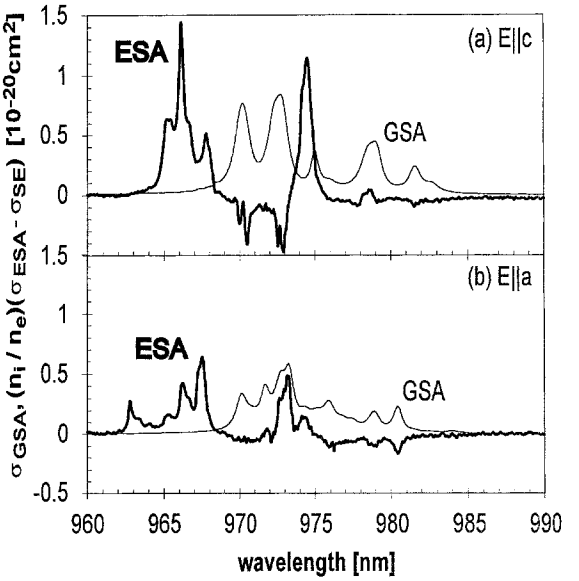

Fig. 5a, b. Polarized spectra at the pump wavelength 970 nm of $Er(5\%):LiYF_4$, (**a**) **E**‖**c**, (**b**) **E**‖**a**: GSA $^4I_{15/2} \rightarrow {}^4I_{11/2}$ and ESA $^4I_{11/2} \rightarrow {}^4F_{7/2}$

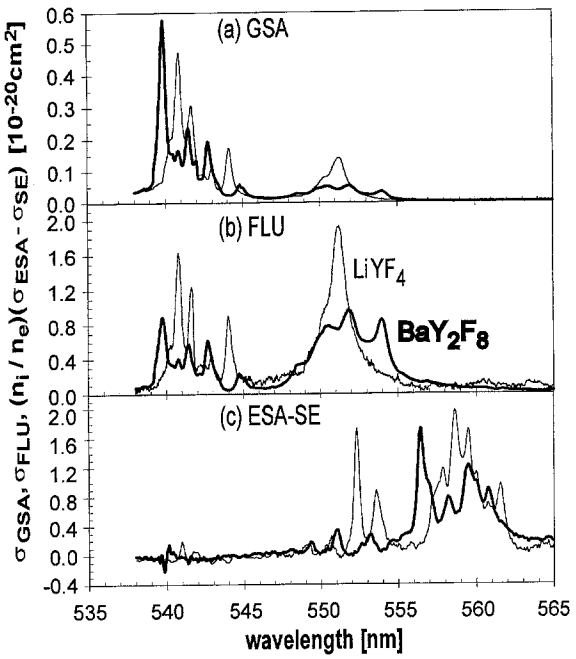

Fig. 6a–c. Polarized spectra at the laser wavelength 550 nm of $Er(7.5\%):BaY_2F_8$, **E**‖**y**, and $Er(5\%):LiYF_4$, **E**‖**c**: (**a**) GSA $^4I_{15/2} \rightarrow {}^4S_{3/2}$, (**b**) fluorescence $^4S_{3/2} \rightarrow {}^4I_{15/2}$, (**c**) ESA $^4I_{13/2} \rightarrow {}^2H_{9/2}$ and $^4I_{11/2} \rightarrow {}^2K_{15/2} + {}^2G_{9/2}$

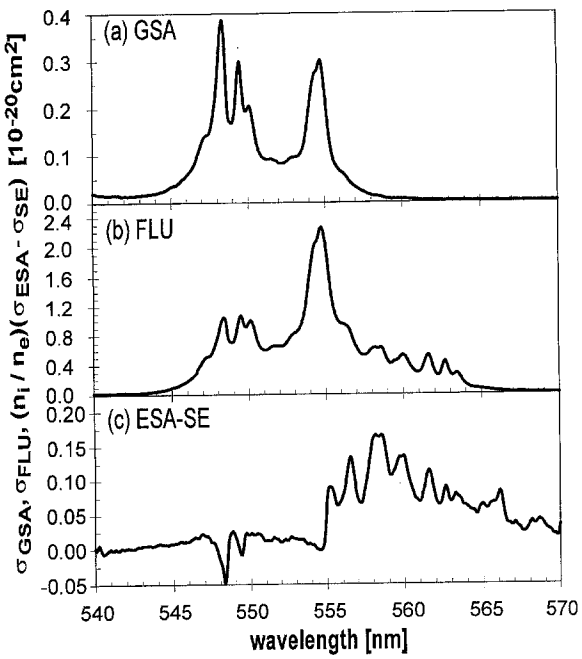

Fig. 7a–c. Arbitrarily polarized spectra of $Cs_3Er_2Br_9$ at the possible laser wavelength 550 nm: (**a**) GSA $^4I_{15/2} \rightarrow {}^4S_{3/2}$, (**b**) fluorescences $^4S_{3/2} \rightarrow {}^4I_{15/2}$ and $^2H_{9/2} \rightarrow {}^4I_{13/2}$, (**c**) ESA $^4I_{13/2} \rightarrow {}^2H_{9/2}$

The labelling of the crystal axes requires some comment, in view of the several conventions employed in the literature. We have chosen in this work to use the designations specified by Jenssen et al. [17]. This is different from that used by Guilbert et al. [18] and appears to imply some confusion concerning real lattice and reciprocal lattice directions derived from X-ray Laue photographs as well as differences in how one chooses to label indices of refraction from high to low values in sequence. We here label the axis of the index ellipsoid as **y** for the direction parallel to the twofold crystal axis [0 1 0]. The **z** axis of the index ellipsoid is approximately 21° from the crystal **c** axis [0 0 1] and the **x** axis of the index ellipsoid is approximately 12° rotated in the same direction from the crystal **a** axis [1 0 0]. The designations used in [4] are such that the equivalent designations are: axis "1" is **z**, axis "2" is **y**, and axis "3" is **x** in the Jenssen convention. A typographical error in [4] needs to be corrected in which axis "1" rather than the incorrect axis "3" is noted to be rotated 21° from the crystal **c** axis [0 0 1].

In a computer simulation using the $Er^{3+}:LiYF_4$ rate-equation system [19] and the parameters of the present pump- and probe-beam experiment, the population mechanisms of $Er^{3+}:LiYF_4$ and $Er^{3+}:BaY_2F_8$ are investigated under 800 nm pumping. This is done in order to estimate the relative population of the $^4I_{11/2}$ level for the determination of SE at 970 nm and the correction of the GSA bleaching as explained in the last paragraph of Sect. 1. Although the lifetime of the $^4I_{11/2}$ level is shorter than the lifetime of the $^4I_{13/2}$ level, approximately 60% of the excitation induced by the pump beam are accumulated in the $^4I_{11/2}$ level. This is mainly due to the small branching ratio on the $^4I_{11/2} \rightarrow {}^4I_{13/2}$ transition which leads to a week feeding of the $^4I_{13/2}$ level [19]. The $^4I_{11/2}$ population results in SE $^4I_{11/2} \rightarrow {}^4I_{15/2}$ around 970 nm in the corrected spectrum, see Figs. 4 and 5. The relative population of the $^4S_{3/2}$ level is small under 200 mW cw pumping and no SE on the transition $^4S_{3/2} \rightarrow {}^4I_{15/2}$ is observed, (Fig. 6c).

In $Cs_3Er_2Br_9$, the determination of the excited-state densities is very complicated, because the parameters for the interionic processes are not known. A computer simulation may, therefore, be misleading in the case of $Cs_3Er_2Br_9$. The $^4S_{3/2}$ level is populated via upconversion, see Fig. 3. This may lead to SE in the measured ESA/SE spectrum, (Fig. 7c). The $\ln(I_u/I_p)$ spectrum is corrected in such a way that the occurrence of SE in the ESA/SE spectrum is minimized.

3 Discussion

3.1 BaY_2F_8 and $LiYF_4$

The suitability of erbium for green laser emission has been investigated in many host crystals, e.g., [1–8]. So far only $LiYF_4$ exhibited a satisfying performance at room temperature under Ti: sapphire pumping [6]. The characteristic properties of $LiYF_4$ can be summarized as follows (cf. also [6, 8, 9]): (1) high absorption cross sections at 970 nm with a fairly good overlap of GSA and ESA at 974 nm in polarization **E**‖**c**, Fig. 5a, (2) a high emission cross section into the upper Stark level of the ground state at 551.2 nm, Fig. 6b, (3) a relatively strong Stark splitting of the ground state, a small Boltzmann population of the terminating laser level, and, consequently, a small reabsorption from the ground state at 551.2 nm, Fig. 6a, (4) an extremely small cross section on the parasitic ESA transition

$^4I_{13/2} \rightarrow {}^2H_{9/2}$ at 551.2 nm, Fig. 6c, and (5) no overlap with the strong ESA $^4I_{11/2} \rightarrow {}^2K_{15/2} + {}^2G_{9/2}$ which dominates the spectrum at wavelengths longer than 556 nm, Fig. 6c.

For erbium in BaY_2F_8 the points 3, 4, and 5 are matched as can be seen by the direct comparison of GSA, fluorescence, and ESA for BaY_2F_8 and $LiYF_4$ in Fig. 6. Unfortunately the emission cross section is lower by a factor of two in BaY_2F_8, Fig. 6b. This will significantly increase the pump threshold for laser emission. On the other hand, in polarization $\mathbf{E} \| \mathbf{y}$, there is a perfect overlap of GSA and ESA at the pump wavelength 969 nm (Fig. 4a). This will lead to an increased pump efficiency. In addition, the lifetime of the $^4S_{3/2}$ upper laser level is longer in BaY_2F_8 (630 μs) than in $LiYF_4$ (400 μs). Both facts may partly compensate for the lower emission cross section.

3.2 $Cs_3Er_2Br_9$

The difference between this material and common oxide and fluoride crystals is mainly induced by the larger size and higher atomic weight of the bromide ions compared to the oxide and fluoride ions. The larger size widens the lattice and weakens the electric crystal field that is induced at the rare-earth site by the Br^- ligands. The high atomic weight limits the energetic spectrum of the lattice vibrations. This leads to the following characteristic differences between $Cs_3Er_2Br_9$ and the fluoride systems.

The weak electric field that is present at the erbium site in $Cs_3Er_2Br_9$, compared to oxide and fluoride ions, reduces the Stark splitting of every level, cf. the wavelength ranges of GSA and fluorescence in Figs. 6a, b and 7a, b. Since the $^4S_{3/2}$ upper laser level has only two Stark levels with a small energetic splitting, this level is hardly affected. The ground state, however, experiences a strong reduction in the Stark splitting from roughly 400 cm^{-1} in the investigated fluoride hosts to 239 cm^{-1} in $Cs_3Er_2Br_9$ [11]. This leads to an enhancement of the Boltzmann population of the terminating Stark laser level in $Cs_3Er_2Br_9$ and a reduction of the inversion that is available at room temperature, cf. the GSA cross sections in Figs. 6a, 7a at the strong fluorescence peaks around 550–555 nm, Figs. 6b, 7b. The emission cross section in $Cs_3Er_2Br_9$, however, is comparable to $LiYF_4$.

On the other hand, the smaller Stark splitting also shifts the wavelength range of parasitic ESA on the transition $^4I_{13/2} \rightarrow {}^2H_{9/2}$ towards longer wavelengths. This ESA limits laser operation in $YAlO_3$ to cryogenic temperatures [7]. In $LiYF_4$ a strong peak of this ESA transition is located a few tenth of a nm from the lasing peak, see Fig. 6b, c, and reabsorption is avoided. In host crystals with large anions like $Cs_3Er_2Br_9$, the parasitic ESA is systematically avoided, because there is no spectral overlap between fluorescence $^4S_{3/2} \rightarrow {}^4I_{15/2}$ and ESA $^4I_{13/2} \rightarrow {}^2H_{9/2}$ (Fig. 7b, c).

The population dynamics of rare-earth ions in oxide and fluoride crystals is dominated by electron-phonon interactions which lead to fast deexcitation processes if the energy gap between two interacting levels can be bridged by a few phonons. Thus the excitation of ions into one level causes a cascade of multiphonon relaxations which produces a population distribution in all lower-lying levels. The highest-phonon energy in $Cs_3Er_2Br_9$ is 190 cm^{-1} [11]. The large number of phonons required to bridge an energy gap of several 1000 cm^{-1} leads to a low probability for this process to occur and results in the almost complete absence of multiphonon transitions even at room temperature. This feature heavily affects the population dynamics of the whole system. The intrinsic lifetime of the $^4I_{9/2}$ level, e.g., is increased from a few μs in fluoride hosts (Fig. 2) to 8 ms in the bromide system (Fig. 3), which was measured in $Er^{3+}(1\%):Cs_3Lu_2Br_9$ [16]. Pumping this level does not lead to the population of the $^4I_{11/2}$ level via multiphonon relaxation as it does in high-phonon hosts. Instead a considerable population is created in the pump level itself which is then subject to interionic energy transfer (Fig. 3). The occurrence of these ion-ion interactions is supported by the close proximity of two erbium ions in the $Cs_3Er_2Br_9$ lattice [11] and by the high erbium concentration of 3.8×10^{21} cm^{-3}.

In the spectral range around 550 nm not only GSA (Fig. 7a) and fluorescence (Fig. 7b) on the transition $^4I_{15/2} \leftrightarrow {}^4S_{3/2}$ and ESA $^4I_{13/2} \rightarrow {}^2H_{9/2}$ (Fig. 7c) are detected. In addition, the inverse process of the ESA, the fluorescence $^2H_{9/2} \rightarrow {}^4I_{13/2}$, is observed (Fig. 7b), because the $^2H_{9/2}$ level is populated via an upconversion process [11] from the pump level (Fig. 3) and is not quenched by multiphonon relaxation. The spectrum shown in Fig. 7b is calculated for correct cross sections on the transition $^4S_{3/2} \rightarrow {}^4I_{15/2}$. The populations of the $^2H_{9/2}$ and $^4S_{3/2}$ levels are different and, therefore, the cross sections of the fluorescence $^2H_{9/2} \rightarrow {}^4I_{13/2}$ include an additional factor. This fluorescence cannot be seen as SE in the ESA/SE spectrum (Fig. 7c). The $^4I_{13/2}$ level is higher populated than the $^2H_{9/2}$ level. The $^4I_{13/2} \leftrightarrow {}^2H_{9/2}$ transition is, therefore, detected as an ESA process in Fig. 7c. The peaks of fluorescence and ESA in the wavelength range 556–564 nm are at the same positions which proves that the same transition is detected in emission (Fig. 7b) and absorption (Fig. 7c).

The ESA from the $^4I_{11/2}$ level at the pump wavelength 970 nm could not be measured in $Cs_3Er_2Br_9$. Under 800 nm excitation the multiphonon transition from the $^4I_{9/2}$ pump level is absent. The $^4I_{11/2}$ level is not sufficiently populated and ESA from this level cannot be detected. The direct excitation at 970 nm would lead to a significant population of the $^4I_{11/2}$ level. The sensitivity of the measuring method, however, does not permit an accurate measurement if scattered laser light is in the spectral range of detection. Another attempt is to excite the $Cs_3Er_2Br_9$ crystal at 488 nm into the $^4F_{7/2}$ level which has a long lifetime in $Cs_3Er_2Br_9$ and to exploit the possible cross relaxation $^4F_{7/2} + {}^4I_{15/2} \rightarrow {}^4I_{11/1} + {}^4I_{11/2}$ for the population of the $^4I_{11/2}$ level. This attempt failed because the damage threshold of the $Cs_3Er_2Br_9$ sample under 488 nm radiation was reached. The small population of the $^4I_{11/2}$ level under 800 nm excitation is also the reason why the strong ESA $^4I_{11/2} \rightarrow {}^2K_{15/2} + {}^2G_{9/2}$ (Fig. 2) that is observed at wavelengths longer than 560 nm in $YAlO_3$ [7] as well as BaY_2F_8 and $LiYF_4$ (Fig. 6c) is completely missing in $Cs_3Er_2Br_9$ (Fig. 7c).

4 Conclusions

The ground-state absorption, fluorescence, and excited-state absorption spectra at the erbium laser wavelength 550 nm have been measured in the host crystals BaY_2F_8, $LiYF_4$, and in $Cs_3Er_2Br_9$. In addition the overlap of GSA and ESA at the pump wavelength 970 nm has been investigated in BaY_2F_8 and $LiYF_4$. The spectral results and the observed population mechanisms are comparable in BaY_2F_8 and $LiYF_4$. Since $LiYF_4$ exhibits good laser characteristics at room temperature a similar performance is expected for BaY_2F_8, with increased threshold vs absorbed pump power but higher absorption efficiency.

Owing to the large size and weight of the anion, the population mechanisms and the spectral properties at the green wavelength range are completely different in $Cs_3Er_2Br_9$. Reabsorption of laser light by parasitic ESA is avoided by a systematic wavelength shift of the ESA due to the smaller crystal field at the erbium site. The same mechanism is responsible, however, for a higher population of the terminating laser level and a smaller inversion on the laser transition. The emission cross section at 550 nm is comparable to $LiYF_4$. The population mechanisms and lifetimes are dominated by fluorescence decay as well as specific interionic upconversion and cross-relaxation processes that have not been observed in oxide and fluoride hosts. Multiphonon relaxations do not significantly contribute to the dynamics of the various levels. Low damage thresholds under Ar^+ and Ti: sapphire radiation may prevent this crystal from lasing at room temperature.

Acknowledgements. The authors thank Stefan Kück and Simone Hartung from the University of Hamburg, Germany, for helpful discussions concerning the experimental arrangement. Mathias Wickleder and Christian Wyss from the University of Bern, Switzerland, are thanked for technical assistance. This work was supported in part by the Swiss Priority Program "Optique". The work of R. A. McFarlane was supported in part by the US Air Force Office of Scientific Research under Contract No. F49620-94-C-0018.

References

1. P. Xie, S.C. Rand: Opt. Lett. **17**, 1198 (1992)
2. R.R. Stephens, R.A. McFarlane: Opt. Lett. **18**, 34 (1993)
3. R. Scheps: IEEE J. QE-**31**, 309 (1995)
4. R.A. McFarlane: J. Opt. Soc. Am. B **11**, 871 (1994)
5. R. Brede, T. Danger, E. Heumann, G. Huber, B.H.T. Chai: Appl. Phys. Lett. **63**, 729 (1993)
6. F. Heine, E. Heumann, P. Möbert, G. Huber, B.H.T. Chai: In *Advanced Solid-State Lasers*, OSA Tech. Dig. (Optical Society of America, Washington, DC 1995) pp. 267–269
7. M. Pollnau, E. Heumann, G. Huber: J. Lumin. **60/61**, 842 (1994)
8. T. Danger, J. Koetke, R. Brede, E. Heumann, G. Huber, B.H.T. Chai: J. Appl. Phys. **76**, 1413 (1994)
9. M. Pollnau, W. Lüthy, H.P. Weber: J. Appl. Phys. **77**, 6128 (1995)
10. D.S. Knowles, H.P. Jenssen: IEEE J. QE-**28**, 1197 (1992)
11. M.P. Hehlen, K. Krämer, H.U. Güdel, R.A. McFarlane, R.H. Schwartz: Phys. Rev. B **49**, 12475 (1994)
12. S. Zemon, G. Lambert, W.J. Miniscalco, R.W. Davies, B.T. Hall, R.C. Folweiler, T. Wei, L.J. Andrews, M.P. Singh: SPIE Proc. **1373**, 21 (1990)
13. J. Koetke, G. Huber: Appl. Phys. B **61**, 151 (1995)
14. M. Pollnau, E. Heumann, G. Huber: Appl. Phys. A **54**, 404 (1992)
15. J. Rubin, A. Brenier, R. Moncorgé, C. Pedrini: J. Lumin. **36**, 39 (1986)
16. M.P. Hehlen, G. Frei, H.U. Güdel: Phys. Rev. B **50**, 16264 (1994)
17. K.M. Dinndorf, D.S. Knowles, M. Gojer, H.P. Jenssen: In *OSA Proc. Adv. Solid State Lasers*, ed. by L.L. Chase, A.A. Pinto (Optical Society of America, Washington, DC 1992) pp. 270–274
18. L.H. Guilbert, J.Y. Gesland, A. Bulou, R. Retoux: Mater Res. Bull. **28**, 923 (1993)
19. M. Pollnau, Th. Graf, J. Balmer, W. Lüthy, H.P. Weber: Phys. Rev. A **49**, 3990 (1994)